Published in final edited form as:

J Mol Biol. 2022 March 15; 434(5): 167451. doi:10.1016/j.jmb.2022.167451.

Identification and characterization of the interaction between the methyl-7-guanosine cap maturation enzyme RNMT and the cap-binding protein eIF4E

Michael J. Osborne[a], **Laurent Volpon**[a], **Mina Memarpoor-Yazdi**[a], **Shubhadra Pillay**[a,e], **Aksharh Thambipillai**[a], **Sylwia Czarnota**[a], **Biljana Culjkovic-Kraljacic**[a], **Christian Trahan**[b,c], **Marlene Oeffinger**[b,c,f], **Victoria H. Cowling**[d], **Katherine L. B. Borden**[a,*]

[a]Institute of Research in Immunology and Cancer, Department of Pathology and Cell Biology, Université de Montréal, Pavilion Marcelle-Coutu, Chemin Polytechnique, Montréal, QC H3T 1J4, Canada;

[b]Department for Systems Biology, Institut de Recherches Cliniques de Montréal, Montréal, QC H2W 1R7, Canada;

[c]Département de Biochimie et Médecine Moléculaire, Université de Montréal, Montréal, QC H3T 1J4, Canada;

[d]Centre for Gene Regulation and Expression, School of Life Sciences, University of Dundee, Dundee, UK, DD1 5EH

[e]current address: Department of Biological Chemistry, Michigan Medicine, University of Michigan, Ann Arbor, Michigan 48109, United States

[f]Division of Experimental Medicine, McGill University, Montréal, QC, Canada;

Abstract

The control of RNA metabolism is an important aspect of molecular biology with wide-ranging impacts on cells. Central to processing of coding RNAs is the addition of the methyl-7 guanosine (m^7G) "cap" on their 5' end. The eukaryotic translation initiation factor eIF4E directly binds the m^7G cap and through this interaction plays key roles in many steps of RNA metabolism including nuclear RNA export and translation. eIF4E also stimulates capping of many transcripts through its ability to drive the production of the enzyme RNMT which methylates the G-cap to form the mature m^7G cap. Here, we found that eIF4E also physically associated with RNMT in human cells. Moreover, eIF4E directly interacted with RNMT *in vitro*. eIF4E is only the second protein reported to directly bind the methyltransferase domain of RNMT, the first being its co-factor RAM. We combined high-resolution NMR methods with biochemical studies to define the binding interfaces for the RNMT-eIF4E complex. Further, we found that eIF4E competes for RAM binding to RNMT and conversely, RNMT competes for binding of well-established eIF4E-binding partners such as the 4E-BPs. RNMT uses novel structural means to engage eIF4E. Finally, we observed that m^7G cap-eIF4E-RNMT trimeric complexes form, and thus RNMT-eIF4E complexes

*correspondence should be addressed to: katherine.borden@umontreal.ca.

may be employed so that eIF4E captures newly capped RNA. In all, we show for the first time that the cap-binding protein eIF4E directly binds to the cap-maturation enzyme RNMT.

Keywords

m^7G capping; RNA maturation; translation; RNA export; RAM

Introduction

RNA maturation and processing are key determinants of ultimate protein function since they impact the composition and biochemical activity of coding RNAs. Methyl-7 guanosine (m^7G) "cap" addition to the 5' end of coding RNAs and many non-coding transcripts is considered the first step in RNA maturation and its efficiency is considered to impact virtually all subsequent levels of their processing[1–3]. Conventional wisdom holds that capping is a constitutive housekeeping activity with the expectation that 100% of coding RNAs would be capped after the first 20–30 nucleotides have been transcribed. In this model, removal of caps by "decapping" inextricably leads to RNA decay. However, new methodologies [4, 5] based on measuring capping on a per transcript basis have demonstrated that m^7G capping is dynamic. Interestingly, RNAs without an m^7G cap are more abundant than previously thought [2, 3, 5–11] and the extent of capping for a given RNA population varies and this is influenced by development, differentiation or oncogene expression[5, 9, 12–14]. Moreover, once capped, RNAs can be decapped and then recapped[6, 8, 15]. In this way, cap removal does not inevitably drive decay. This has led to the notion of cap homeostasis, whereby the cap status of transcripts can be regulated to impact RNA export, translation, stability *etc* [6]. Consistent with this model, genome-wide studies suggest that uncapped RNAs are more stable than anticipated and in this way [4], cap status can be a means to titrate transcript activity as well as their capacity to undergo other processing steps.

The addition of the m^7G cap is a three-step process involving RNGTT (RNA guanylyltransferase and 5' phosphatase) and RNMT (RNA guanine-7-methyltransferase) in mammals [16]. These enzymes are required for capping and cell survival[2, 17–23]. The final step is methylation of the cap guanlylate by RNMT and utilizes S-adenosyl methionine (SAM) as the methyl donor [24, 25]. RNMT also binds a small co-factor protein, RAM which increases its methylation activity by up to four-fold and additionally can recruit RNAs to the complex [24, 26]. At steady state, RNMT and RNGTT are predominantly nuclear but are also found at lower levels in the cytoplasm. Indeed, capping activity was directly observed in both the nucleus and cytoplasm [8, 19, 27]. These studies indicate that capping can occur at multiple places in the cell i.e. *de novo* capping which generally occurs co-transcriptionally where RNGTT, RNMT and RAM localize to sites of transcription, as well as re-capping which has been shown in the cytosol and would be predicted to also occur in the nucleus given the presence of these enzymes diffusely throughout the nucleoplasm (not restricted to sites of transcription)[4]. Thus, like splicing and polyadenylation [28–30], capping can occur both co- and post-transcriptionally.

Recent studies with the eukaryotic translation initiation factor eIF4E revealed novel facets for the regulation of capping [5]. eIF4E overexpression is associated with poor prognosis in many cancers [31]. eIF4E directly binds the m^7G cap on specific RNAs to recruit them to the RNA export complex in the nucleus as well as to the ribosome for translation in the cytoplasm [32, 33]. We found that eIF4E increased both the nuclear export and translation efficiency of *RNGTT* and *RNMT* transcripts as well as the nuclear export of *RAM* [5]. Consistently, eIF4E overexpression led to increased levels of RNGTT, RNMT and RAM proteins. In this way, eIF4E could increase production of its m^7G cap substrate. eIF4E increased the percentage of capping for specific RNAs; and indeed, these studies suggested that for many of these RNAs the steady-state levels of capping (30–50%) were much less than anticipated. This mode of regulation is a potentially powerful means to modulate pre-mRNA's protein-coding capacity. Indeed, capping of specific eIF4E-senstive RNAs was observed in high-eIF4E cancer specimens [5]. Clearly the elevation of the capping machinery promoted capping for selected RNAs by eIF4E. Significantly, we also noted that some RNA targets were in both RNMT and eIF4E nuclear RNA immunoprecipitations [5]. This raised the possibility that eIF4E and RNMT could physically interact in cells and perhaps directly associate. In this way, eIF4E could directly modulate capping through a physical interaction with RNMT in addition to its ability to elevate RNMT levels.

In mammalian cells, studies have reported RNMT can bind a number of proteins, namely: the capping machinery (RAM and RNGTT [34]); Importin-alpha, presumably for the nuclear import of RNMT[14, 35]; CDK1-cyclin B, which are involved in phosphorylation of RNMT on its N-terminus[14] and, the PAF transcriptional complex[26]. Of these, only RAM directly bound to, and was stably associated with, RNMT. Here, we demonstrated that eIF4E physically associated with RNMT in mammalian cells and that eIF4E interacted directly with the methyltransferase domain of RNMT by using NMR and biochemical methods. In all, these studies revealed that there is a functional interplay between the enzyme that generates methylated caps, RNMT, and one of the major m^7G cap binding proteins in mammalian cells, eIF4E.

Results.

eIF4E interacts with RNMT but not RAM in human cells

We investigated whether eIF4E physically associated with the capping machinery in human U2OS osteosarcoma cells, which were used extensively to characterize eIF4E's RNA export, translation and more recently capping activity [5, 36–41]. Capping can occur in the nucleus co-transcriptionally and/or post-transcriptionally including in the cytoplasm [4, 6, 8, 15, 27]. As a first step to assess the ability of eIF4E and RNMT to interact in U2OS cells, we assessed the spatial localization of endogenous RNMT and eIF4E using confocal laser microscopy in conjunction with immunofluorescence to detect endogenous proteins (Figure 1A). Micrographs represent single sections through the plane of the cells. eIF4E, in green, was found in both nuclear and cytoplasmic compartments. Within the nucleus, eIF4E was localized in nuclear bodies and in a diffuse localization, as reported previously[38, 40–42]. RNMT, in red, was enriched in the nuclei where it adopted a mainly diffuse localization; and was also present at lower levels in the cytoplasm consistent with previous reports [27].

Given the diffuse nuclear localization, it was not possible to ensure that co-localization (observed in yellow) could be interpreted as interaction, but these experiments did indicate that within intact cells, RNMT and eIF4E were positioned to interact. To assess if these endogenous proteins did indeed interact in cells, we carried out immunoprecipitations using anti-eIF4E antibodies from nuclear lysates employing formaldehyde crosslinking to preserve native interactions (Figure 1B). We observed that eIF4E immunoprecipitated with RNMT as well as the eIF4E binding protein, 4E-BP1 which served as a positive control [43]. eIF4E did not associate with the negative IgG control indicating these associations were specific (Figure 1B). We also observed the RNMT-eIF4E immunoprecipitation in non-crosslinked cells (data not shown). Interestingly, eIF4E did not immunoprecipitate with RAM (Figure 1B). In all, endogenous RNMT and eIF4E are found in overlapping sites in intact cell nuclei and physically interacted in nuclear lysates.

eIF4E directly binds to RNMT

Given the physical association of RNMT and eIF4E in cells, we explored whether these proteins directly interacted using GST-pulldown and NMR methods. We expressed full-length human eIF4E and multiple constructs of human RNMT in *E. coli* (shown schematically in Figure 1C: see Supplementary Fig. S1 for full sequence details). All proteins were purified to homogeneity (Figure 1D). The following RNMT constructs were expressed: the full-length protein (RNMT-FL, 476 residues); the methyltransferase domain consisting of residues 164–476, (referred to RNMT-C hereafter, the structure of which is shown in Figure 1E) and RNMT-C Δlobe in which residues 416–456 of RNMT-C were removed (dark green, Fig 1E)[34]. The RNMT-C construct is comprised of the methyltransferase domain, whereas the “lobe” region within the RNMT-C (residues 416–456) was important for binding of RAM (orange, Figure 1E); and in the absence of RAM this lobe is unstructured[34]. The deletion of the RNMT lobe impairs RNMT methyltransferase activity as well as RAM binding to RNMT[34]. The unstructured N-terminal domain (1–120), which is not shown, is responsible for RNMT recruitment to transcription initiation sites and can impact on RNMT activity by an ill-defined mechanism[14, 44]. The SAM methyl donor binding site of RNMT, defined via crystal structures using the SAH analogue (shown as yellow spheres Figure 1E), is distal to the RAM binding site[34].

GST-pulldown experiments revealed both RNMT-FL and RNMT-C bound to GST-eIF4E beads (Figure 1G). The extent of RNMT binding was highly similar between these RNMT constructs indicating that the N-terminus was dispensable for binding to eIF4E. Similarly, studies with the RNMT-C Δlobe revealed that the lobe was not necessary for eIF4E binding as seen by the similar level of binding to wildtype RNMT-C. Importantly, none of the RNMT constructs bound to GST-beads alone, indicating that the binding of RNMT to eIF4E was specific. ^{1}H-^{15}N HSQC NMR experiments using ^{15}N-labelled eIF4E (50 μM) with the various unlabelled RNMT constructs confirmed these interactions (Figure 1H, Supplementary Fig. S2A,B). Addition of 4-fold excess of RNMT-FL, RNMT-C and RNMT-C Δlobe induced a reduction of the ^{1}H-^{15}N HSQC signals corresponding to the folded regions of eIF4E (quantified in the bar graphs as a reduction in intensity, Figure 1H, Supplementary Fig. S2A,B), consistent with an increase in overall tumbling associated

with the formation of the eIF4E-RNMT complex. We note that changes were similar for all constructs, consistent with GST-pulldown results that the N-terminus and lobe of RNMT were not important for eIF4E recognition. Due to more favourable solution properties of the RNMT-C construct relative to the other constructs, all RNMT experiments hereafter were performed on RNMT-C, unless otherwise stated. We note we did not observe significant changes to the flexible N-terminus of eIF4E (residues 1–36) indicating that this unstructured region remains mobile after association with RNMT i.e. this region did not bind RNMT and remains flexible. In all, our data show eIF4E directly associated with the methyltransferase domain of RNMT.

RNMT binds the dorsal surface of eIF4E and not its cap-binding site

To investigate the binding surface used by RNMT on eIF4E, we first explored whether the m^7GDP cap analogue and RNMT could compete for eIF4E binding; similar experiments have shown the importance of the cap-binding site for eIF4E association with VPg and Importin 8 [45, 46]. Cap recognition for eIF4E is mediated via pi-pi interactions of the m^7G moiety with aromatic rings of W56 and W102 of eIF4E and are further enhanced by favorable electrostatic interactions of the m^7GDP's phosphate groups with the basic residues in eIF4E (K157, K159 and R162) (Figure 1F). Competition experiments were carried out with GST-eIF4E pulldowns (Figure 2A) and ^{1}H-^{15}N HSQC NMR (Figure 2B) experiments in the presence of 20-fold excess of m^7GDP. In both cases the presence of m^7GDP cap did not diminish binding of RNMT to eIF4E. To further investigate the importance of the cap-binding site in RNMT-C recognition of eIF4E, we monitored binding of RNMT-C to a cap-binding mutant of eIF4E (K157E/K159E/R162E). This triple mutant (eIF4E TrMut) abrogated cap-analogue binding as well as binding of proteins (Importin 8 and VPg) that utilize the cap surface to associate with eIF4E ([45, 46]). Indeed, this mutant bound RNMT similarly to wildtype eIF4E as observed by ^{1}H-^{15}N HSQC spectra using the ^{15}N-labelled eIF4E triple mutant and unlabelled RNMT-C (Supplementary Fig. S2C). Thus, our observations show that eIF4E does not utilize its cap-binding surface for RNMT-C association. We note that these experiments do not prove the existence of ternary eIF4E-RNMT-m^7GDP cap complexes, this is addressed in a later section.

The extreme broadening of eIF4E cross-peaks induced by RNMT, as observed in the ^{1}H-^{15}N HSQCs, precluded the use of chemical shift perturbation techniques or the use of distance-based nuclear Overhauser effect (NOE) approaches since the peaks involved in complex formation disappeared. We therefore used transferred cross saturation (TCS) NMR methods [47], which can accurately define residues in contact at a protein-protein surface. In this experiment, deuterated ^{15}N-labelled eIF4E and low ratios of the unlabelled RNMT-C partner protein coupled with TROSY-based NMR detection techniques are used to minimize the deleterious effects of line broadening. In this experiment ^{15}N-^{2}H labeled eIF4E (150 μM) was in excess relative to unlabeled RNMT (110 μM). Experiments were done in the presence m^7GDP ligand (16-fold excess over eIF4E) to reduce aggregation which can be observed more readily in apo-eIF4E samples over time[48]. We note that m^7GDP does not interact with RNMT-C under these conditions as observed by ITC (data not shown) and by cap chromatography (Figure 3A). Unfortunately, high residual proton content in the ^{2}H-^{15}N eIF4E samples resulted in intensity changes in the control experiments on eIF4E alone. We

therefore evaluated residues at the interaction surface by comparison of the intensity ratio (saturated and unsaturated spectra) for eIF4E in the presence and absence of RNMT, similar to methods used in previous reports [49]. Several points, corresponding to eIF4E residues 70, 73, 75 and 81, deviate more than 0.66* 1 standard deviation from the mean (bold middle line) and are known from the structure to be at the surface. All these residues have a lower saturation (I_{on}/I_{off}) ratio (see methods for details) corresponding to stronger cross saturation in the complex compared to eIF4E alone. We note that these residues are located on the first helix of eIF4E, which constitutes part of the dorsal surface (Figure 2 D,E). In contrast, no significant changes are observed for residues in the cap-binding pocket of eIF4E e.g. W56 or W102 (Figure 2 C,D,E), indicating this site was not close in space to RNMT, consistent with our above studies.

To further investigate the eIF4E binding surface, we utilized specific ^{13}C-labelling methods to map the binding site on eIF4E since ^{1}H-^{13}C resonances are less sensitive to global broadening due to tumbling than ^{1}H-^{15}N signals [50]. We prepared an eIF4E sample whereby the δ methyl side chains of Ile (δ1) and Leu (δ1, δ2) and the γ methyls of Val were selectively protonated and ^{13}C-labelled, the remaining protons and carbons were deuterated and ^{12}C-labelled respectively. Assignments for the side-chains of eIF4E were incomplete for apo-eIF4E and not reported for m^{7}GDP- eIF4E, we therefore assigned all ILV methyls that were ^{13}C-labelled (with the exception of Cγ2 of V194) (Supplementary Table S1), and additionally extended the number of assignments for the backbone residues of apo- and cap-bound eIF4E (BMRB 27427 and 27428). With this information in hand, we monitored these methyl groups in the ^{1}H-^{13}C HSQC as a function of RNMT-C addition. Here, unlabelled RNMT-C was added at a 0.5:1 molar ratio (25 μM RNMT-C: 50 μM ILV eIF4E) or, using a separate preparation of proteins, at a 3.8:1 molar ratio of RNMT-C (190 μM) to eIF4E (50 μM) (Figure 2F). The same resonances were broadened in both cases with effects more pronounced at the higher molar ratio of RNMT-C to eIF4E. The apo-eIF4E spectra is shown in red and with RNMT-C, in green. The extent of broadening of these methyl groups are highlighted in yellow on the apo-eIF4E structure, where the size of the methyl sphere reflects the extent of broadening. Methyl groups on the dorsal surface of eIF4E exhibited substantial broadening (V69, I98, V182, L187) as well as to a lesser extent in the hydrophobic core near to these surface residues (L45, L75, L85, L93, L137, V149, V176). Consistent with the above data, there was no significant broadening of ILV residues in the cap-binding site. Overall, our NMR data define the dorsal surface of eIF4E as the RNMT-binding site and indicate the cap-binding site of eIF4E is dispensable for the interaction.

Given RNMT binds at the dorsal surface of eIF4E, and does not compete for binding with cap, we next sought to understand if trimeric complexes of cap-eIF4E-RNMT could form using m^{7}G cap chromatography experiments (Figure 3A). Here, eIF4E or RNMT-C alone or in combination were incubated with m^{7}G cap beads. RNMT-C did not bind to m^{7}G cap beads while eIF4E readily did. This is consistent with previous studies that demonstrated that RNMT had very low affinity for its enzymatic product the methylated cap [25, 35]. The addition of RNMT-C in the presence of eIF4E led to capturing of RNMT-C onto the m^{7}G cap beads. This indicated that trimeric complexes of cap-eIF4E-RNMT form. Taken together, our studies demonstrated that eIF4E-m^{7}G cap can complex with RNMT

through the dorsal surface of eIF4E. Further, they showed that RNMT-C association does not substantially affect the ability of eIF4E to bind to m^7GDP.

eIF4E and RAM compete for RNMT

Next, we investigated whether eIF4E competed for the RAM-binding site on RNMT. RAM is not stable alone and thus was co-purified with RNMT-C. The complex was purified to homogeneity as described in [24]. GST pulldown competition experiments showed that the presence of RAM abrogated binding of RNMT-C to GST-eIF4E beads relative to RNMT-C alone (Figure 3B). This strongly suggested that eIF4E and RAM recognized an overlapping surface on RNMT-C (Figure 1C). Notably, the RAM-binding site does not overlap the SAM or Gppp binding sites on RNMT-C, suggesting that the catalytic site is not implicated in the interaction with eIF4E. Given that RAM and eIF4E competed for RNMT-C, we used the RNMT-C/RAM co-structure to guide our mutation strategy. In this structure, RAM adopts an elongated, helical conformation binding a long, narrow surface of RNMT-C including its flexible lobe (Figure 1C)[34]. Our pulldowns and NMR data (Figure 1G,H; Supplementary Fig. S2B) showed that the RNMT lobe was dispensable for eIF4E binding and therefore we designed a series of mutations for RNMT based on the interface with the first two helices of RAM and connecting loop (Figure 3C). We started by introducing multiple mutations to interrogate this surface on RNMT-C more efficiently. Mutants of RNMT-C residues that interact with both helices: F322A/E323A/R326A/Y374A, showed a decrease in binding to eIF4E (Supplementary Fig. S3A). We then examined the impact of multiple mutations at the RNMT-C binding site for the first RAM helix (L353A/Y374A and N379A/E380K/K383E) which substantially reduced binding; by contrast, RNMT-C residues at the site of the second RAM helix F322A/E323A/R326A/K392E (Supplementary Fig. S3A) and F322A/E323A (Figure 3D) did not substantially impact the interaction with eIF4E. Further mapping highlighted that single point mutations (Y294A, Y374A or E380K, coloured red in Figure 3C) were sufficient to abrogate the RNMT-C interaction with eIF4E (Figure 3D). Importantly, mutants did not lead to unfolding of RNMT-C as observed by circular dichroism studies (Supplementary Fig. S3B). This data revealed that the eIF4E-binding site on RNMT-C involves the beginning of helix D (Y294) and helix F (Y374, 380) with contributions possibly from the loop connecting β-strands 7 and 8 (Y353) (Figure 3C). Consistent with the RAM competition studies (Figure 3B), the eIF4E-binding site on RNMT-C partially overlaps the RAM-binding site. To further define the RNMT surface, we generated ^{1}H-^{15}N labelled RNMT-C samples. However, we were unable to obtain solution conditions that produced the necessary protein stability for assignment of RNMT-C resonances and thus, could not perform similar experiments with labelled RNMT and unlabelled eIF4E. In all, eIF4E binds to RNMT in a site that partially overlaps with the RAM-binding site.

Given previous studies demonstrated that RAM stimulated the methyltransferase activity of RNMT by about 4-fold [24, 34], we examined if eIF4E had a similar activity. Using eIF4E concentrations ranging from 0–80 μM and 20 μM RNMT-C, we monitored the capping of an *in vitro* transcribed ^{32}P- Gppp 55-base oligoribonucleotide in the presence of the methyl donor SAM as described in[34]. The RNMT-C construct displayed methyltransferase activity. However, we noted that eIF4E addition did not impact levels of methylated cap

produced (data not shown). This may be because eIF4E does not bind to the lobe which is critical for RAM-mediated enhancement of RNMT activity [24, 26], or that eIF4E requires a co-factor to modulate the methyltransferase activity of RNMT, likely one that binds the lobe, that is present in cells but not in our assays. Alternatively, eIF4E may simply not modulate RNMT's enzymatic activity.

Structural model of the eIF4E-RNMT complex

To generate a structural model for the complex of RNMT-C with eIF4E, we used the above experimentally determined restraints as input into the molecular docking software Haddock[51]. Restraints included TCS and ^{13}C-methyl broadening data for eIF4E residues as well as mutational data for RNMT-C. Out of the 200 water-refined models, 8 clusters were obtained. The largest cluster (containing 84 structures) was the only one exhibiting a Z-score below the −1 threshold (−1.7), and a Haddock score below −100 threshold (−110). This cluster was characterized by highly convergent poses (Supplementary Fig. S4). The pose with the lowest energy is shown in Figure 3E–G. Consistent with the input restraints, eIF4E employs its dorsal surface, most notably helices 1 and 2 to interact with the portion of the RAM-binding site on RNMT-C that does not involve the lobe (helices D and F) (Figure 3E). The complex interface is also far removed from the RNMT catalytic site. This model is consistent with several biochemical observations that were not used as restraints for the model. For instance, mutation of the cap-binding site of eIF4E has no effect on association with RNMT-C (Supplementary Fig. S2C), m^{7}G cap analogues do not compete for the interaction of RNMT with eIF4E (Figure 2A, B) and RNMT-C/eIF4E-cap complexes can be observed (Figure 3A); and consistently in this model, RNMT does not bind to the cap-binding site of eIF4E. Indeed, binding of eIF4E dorsal surface partners (eIF4E-BP1 and BP2) compete for RNMT-C binding to eIF4E (see below; Figure 4A) consistent with our model when overlaid with coordinates for the eIF4E-BP1 complex (Figure 3G). Similarly, the deletion of the lobe in RNMT-C has no impact on eIF4E binding (Figure 1G, Supplementary Fig. S2B) and is not used by eIF4E to bind RNMT-C in this model. Furthermore, the RAM-binding site overlaps with the one predicted for eIF4E binding on to RNMT-C (Figure 3F) consistent with eIF4E competition for RAM binding to RNMT-C (Figure 3B). While RAM and eIF4E compete for overlapping sites on RNMT-C, specifically helix 1, there is no similarity between the orientation of the RAM helix with helices 1 or 2 of eIF4E at the RNMT-C surface in our model; however, high-resolution structural studies would be needed to be definitive about these orientations. Finally, the binding regions of RNMT-C and eIF4E both consist of hydrophobic patches suggesting that electrostatics do not play a major role in this interaction (Supplementary Fig. S5).
In parallel, we conducted cross-link mass spectrometry (XLMS) on recombinant, purified heterodimers to further study the complex. As predicted by the Haddock models, the eIF4E interface used by RNMT-C is lysine poor, explaining the paucity of high confidence cross-links at the interface between eIF4E and RNMT. In all, the eIF4E/RNMT-C complex model is consistent with our biochemical and NMR studies.

eIF4E-RNMT complexes are distinct from eIF4E RNA export or translation complexes

eIF4E is known to exist in several complexes within cells. The best characterized are its translation and RNA export complexes[33, 52]. The dorsal surface of eIF4E is recognised

by key components of these translation and RNA export complexes, including LRPPRC, eIF4G and the eIF4E binding proteins (4E-BPs). Given the above data, one would predict that the RNMT-eIF4E complex is biochemically distinct from these previously identified complexes, since all of these complexes compete for overlapping portions of the dorsal surface of eIF4E. To examine this possibility, we generated purified proteins and used GST pulldowns (Figure 4A,B). In all cases, the eIF4E-partner protein was preincubated with GST or GST-eIF4E beads followed by addition of RNMT-C. Starting with factors relevant to eIF4E's role in translation, we used a purified peptide corresponding to the binding site of eIF4E's translation co-factor the 220 kDa eIF4G1 to eIF4E and refer to this peptide as 4Gp. We also examined two negative regulators of eIF4E-dependent translation which coopt the eIF4G-binding site on eIF4E: full-length 4EBP1 and 4EBP2 proteins [33]. In all cases, preincubation of 4EBP1/4EBP2 proteins or 4Gp with GST-eIF4E, impaired the binding of RNMT-C to GST-4E beads relative to GST-eIF4E beads alone. We note that RNMT-C, 4EBP1 and 4EBP2 did not bind to the GST negative control (Figure 4A,B, Supplementary Fig. S6). We note that, the 4EBPs were produced in bacteria and thus are not phosphorylated; however, given phosphorylation of 4EBPs reduces their affinity for eIF4E [53], their phosphorylation would make RNMT an even more effective competitor. In parallel, we similarly examined the RNA export co-factor LRPPRC which directly binds eIF4E and CRM1[39, 52]. Here, we show that LRPPRC cannot bind to eIF4E in the presence of RNMT-C (Figure 4B), suggesting that at least in these *in vitro* conditions, RNMT-C has a stronger affinity for eIF4E than does LRPPRC. In all, RNMT-C binds to the dorsal surface at a site overlapping the 4Gp, 4EBP1, 4EBP2 and LRPPRC-binding sites on eIF4E consistent with our above NMR data. These findings indicate that RNMT-eIF4E complexes are biochemically distinct from eIF4E's translation and RNA export complexes.

Discussion

Our previous studies showed that eIF4E overexpression drove the production of the capping machinery including RNMT and RAM[5]. This was achieved through eIF4E's ability to promote the nuclear export of *RNMT, RNGTT* and *RAM* transcripts and translation of *RNMT* and *RNGTT* transcripts. This elevation was associated with increased m^7G capping efficiency for a subset of RNAs. Indeed, RNA immunoprecipitations showed that eIF4E and RNMT bound to overlapping RNA populations in cells [5]; however, whether these bind to the same RNA molecule at the same time is not yet known, but in such cases, this may rely on the recently reported ability of RNMT to also bind the body of RNAs [26].

These observations revealed, for the first time, a possible functional interplay between RNMT and eIF4E. Here, we demonstrated that eIF4E physically associated with RNMT in cells, and directly bound to RNMT *in vitro*. The interactions between eIF4E and RNMT highlight novel ways to engage both proteins. Our data support models whereby eIF4E binds to helices D and F on RNMT, distal to its catalytic site. The eIF4E-binding site overlaps with that used by RAM, and indeed, our studies show eIF4E competes for RAM-binding onto RNMT. The dorsal surface of eIF4E is recognized by RNMT. Interestingly, RNMT does not contain the YXXXXLΦ eIF4E-consensus binding motif which is employed by eIF4G or 4E-BPs to bind the dorsal surface[4]. Furthermore, this region of RNMT does not contain any similarity to other motifs known to bind the dorsal surface of eIF4E such as RING

domains [4, 33]. Our studies present the first evidence that eIF4E can bind to any component of the capping machinery, in this case RNMT, which is of particular interest given eIF4E is itself a cap-binding protein.

There are several functional implications related to the identification of eIF4E-RNMT complexes. For instance, the competition between eIF4E and RAM for RNMT may influence which RNA targets have increased capping given RAM also plays a role in RNA recruitment to RNMT. It is interesting that while on the one hand eIF4E competes for RAM binding to RNMT (Figure 3B,F); on the other, eIF4E elevates both RAM and RNMT protein levels[5]. In this way, eIF4E may drive the production of two distinct pools of RNMT in the cell, bound to either RAM or eIF4E. In terms of methyltransferase activity, we did not observe any impacts of eIF4E addition on RNMT capping activity of a model RNA *in vitro*. This could be because eIF4E does not bind the lobe of RNMT and thus does not induce the same conformational changes as those induced by RAM. In cells, eIF4E could recruit factors to the lobe which then promote capping. Future studies are required to dissect these possibilities.

It is tempting to speculate that eIF4E associates with RNMT in order for eIF4E to rapidly bind newly produced m^7G capped RNA (Figure 4C). In this way, once RNMT is remodelled out of the complex, eIF4E could use these RNAs as substrates in the nucleus for RNA export, and in the cytoplasm, for translation (Figure 4C). The relative orientation of the cap-binding site of eIF4E and the catalytic site of RNMT make this at first glance appear less likely to occur, at least in *cis*. However, the close proximity of RNMT, eIF4E and the newly capped RNAs make this a feasible model and such a hand-off could also occur in *trans*. RNMT may also titrate eIF4E's other activities by preventing formation of RNA export or translation complexes *in vitro* by competing with the export and translation machinery (Figure 4C). Given we observe cap-eIF4E-RNMT trimeric complexes, RNMT could sequester eIF4E-RNA complexes in a manner similar to that observed for RNA-eIF4E-BP1 complexes[54, 55]. In this scenario, it seems likely that eIF4E activity would be determined by the relative levels of its binding partners (e.g. eIF4G, LRPPRC, RNMT) which then could recruit eIF4E to corresponding complexes. Additionally, it is also possible that the direct RNMT-eIF4E interaction may be relevant to activities independent of capping, particularly with regard to transcriptional roles for RNMT [26, 44]. Indeed, RNMT has been found to physically associate with RNAs along their entire length [26]. These possibilities require further examination.

In all, we discovered that eIF4E binds to RNMT in cells and directly *in vitro*. We characterized the binding surfaces and unearthed novel structural strategies to engage these proteins. These are the first studies to demonstrate that eIF4E can physically associate with any component of the capping machinery, which is particularly interesting given the chief activity of eIF4E is to bind the RNA cap. These results point to a new biochemical functionality for eIF4E in the nucleus. Indeed, biochemical and cell biological studies demonstrated that eIF4E bound to RNA export complexes constituted of 4ESE-RNA, LRPPRC and CRM1 [52]. Our studies indicate that the eIF4E-RNMT complexes are distinct from the RNA export complex. There are many possible functions for eIF4E-RNMT

complexes as outlined above. In all, our results suggest an unanticipated functional interplay between these cap-generating and cap-binding proteins.

Methods

Cell Culture

U2OS cells (obtained from ATCC) were maintained at 37°C and 5% CO2 in Dulbecco's modified Eagle's medium (DMEM) (ThermoFisher Scientific) supplemented with 10% fetal bovine serum (FBS) (ThermoFisher Scientific) and 1% penicillin-streptomycin (ThermoFisher Scientific). The U2OS cell line was authenticated using STR profiling (Wyndham Forensic Group). Cultured cells were routinely checked to ensure that there was no mycoplasma contamination by PCR[56].

Immunofluorescence and Laser-Scanning Confocal Microscopy

U2OS cells were grown on 4 well glass slides (Millicell EZ SLIDE 4 well glass, Millipore Sigma PEZGS0416). After washing three times in 1× PBS (pH 7.4), cells were fixed in 3% paraformaldehyde for 10 min at room temperature (RT), quenched 5 min with 0.15 M glycine, washed three times with PBS, and permeabilized with 0.5% (vol/vol) Triton X-100 for 10 min at RT. After washing three times in PBS, cells were blocked for 1 h in Blocking solution (10% FBS and 0.1% Tween 20 in PBS), and incubated with primary antibodies diluted in Blocking solution overnight at 4 °C (1:100 mouse anti-eIF4E and 1:500 rabbit anti-RNMT or 1:100 mouse anti-RNMT and 1:500 rabbit anti-eIF4E, or rabbit-anti-RAM 1:500). After washing three times in PBS, cells were incubated with fluorescent-dye conjugated antibodies diluted in Blocking solution for 1 h at RT (1:200 dilution anti-mouse Alexa Fluor 488 and anti-rabbit Alexa Fluor 546, ThermoFisher Scientific). The cells were washed four times with PBS and mounted in antifade mounting medium with DAPI (Vector Laboratories, H-2000). Analysis was carried out using a laser-scanning confocal microscope (LSM700 META; Carl Zeiss, Inc.), exciting 405 nm, 488 nm or 543 nm with 63x oil objective and numerical aperture of 1.4. Channels were detected separately, with no cross talk observed. Confocal micrographs represent single sections through the plane of the cell. Images were obtained from ZEN software (Carl Zeiss, Inc.) and displayed using Adobe Photoshop CS6 (Adobe).

Co-Immunoprecipitation studies

Nuclei isolated using the cellular fractionation protocol were rinsed 2x with 1×PBS and fixed with 1% PFA for 10min at RT with rotation, quenched 5min with 0.15M Glycine (RT with rotation), then washed 3 times with 1×PBS and lysed in 0.5ml NT-2 buffer by 3 times 6 seconds bursts (with 30 second pause between each burst) using microtip at 25% power (Sonic Dismembrator Model 500, Fisher, Max Output 400W). NT-2 buffer: 150mM NaCl, 50mM Tris-HCl (pH 7.4), 2.5mM $MgCl_2$, 0.05% NonidentP-40, 8 supplemented with 1mM DTT, 1x protease inhibitors without EDTA, 200U/ml RNaseOut. Nuclear lysates were centrifuged at 10 000 × g for 10min, and supernatants were transferred into fresh tubes. After adjusting the concentration to be no more than 1mg/ml, nuclear extracts were pre-cleared with 50 μL protein G conjugated superparamagnetic beads (Dynabeads Protein G, ThermoFisher Scientific) for 30 min at 4°C. Pre-cleared lysates were incubated with

10 μg of anti-eIF4E antibody (per 1mg of the lysate) or 10 μg of appropriate IgG as a control, and 0.5 mg/ml yeast tRNA (SigmaAldrich), overnight at 4°C with rotation. Rabbit antieIF4E (RN001P, MBL), mouse anti-eIF4E (A10, Santa Cruz) antibodies were used in this study as indicated in the text. After ON incubation, 50μl of Dynabeads were added and incubated for additional 3h at 4°C with rotation. Beads were washed once with NT-2 buffer supplemented with 1mg/mL heparin (Sigma-Aldrich) for 5min at 4°C with rotation, and an additional six times with NT-2 buffer with 300mM NaCl. After washing, beads were resuspended in 2xLaemmli Buffer with β-mercaptoethanol, and incubated for 5 min at 98°C. Co-immunoprecipitated proteins were resolved on SDS-PAGE and visualized by Western blotting.

Cellular Fractionation

About 3–5 × 10^7 cells were collected and washed twice in ice-cold PBS (300 × g for 3–5 min) and then resuspended with slow pipetting in 0.5 mL of lysis buffer B (10 mM Tris (pH 8.4), 140 mM NaCl, 1.5 mM MgCl2, 0.25% Nonidet P-40, 1 mM DTT, 100 U/mL RNase inhibitors). The lysate was centrifuged at 1000 × g for 3 min at 4°C, and supernatant (cytoplasmic fraction) was transferred into a fresh microtube. The pellet (nuclear fraction) was resuspended in 1 Volume of lysis buffer B and transferred to a round-bottomed polypropylene tube, and 1/10 volume of detergent stock (3.3% sodium deoxycholate, 6.6% Tween 40 in DEPC H2O) was added with slow vortexing (to prevent the nuclei from clumping) and incubated on ice for 5 min. The suspension was transferred to a microtube and centrifuged at 1000 × g for 3 min at 4°C. Supernatant (post-nuclear fraction) was cytoplasmic fraction.

Protein Purification

Recombinant human eIF4E (gift from Dr N. Shimma, *Chugai Pharmaceutical Co.*, Japan) was inserted into the pET-28a vector between the BamHI and XhoI restriction sites. In addition, a TEV protease cleavage site was inserted between the T7 tag and eIF4E leaving the sequence Gly-Ser attached to the N-terminus of the protein. The plasmid was overexpressed in *Escherichia coli* BL21(DE3) cells in LB rich medium at 37°C and induced overnight by 0.5 mM isopropyl-*β*-D-thiogalactopyranoside (IPTG) at 30°C. Expression of uniformly labelled ^{15}N and $^{15}N/^{13}C$ protein was performed in M9 minimal media containing 2g/L ^{15}N ammonium chloride and 2g/L $^{13}C_6$ glucose as the sole nitrogen and carbon sources. Cells were harvested by centrifugation and stored at −20°C until use. The frozen cells were resuspended in PBS buffer supplemented with 300mM NaCl, 7mM β-mercaptoethanol (βME), 0.5% Igepal, 1mg/ml lysozyme, cocktail of protease inhibitor (GE), 10mM imidazole, and lysed by sonication on ice (Sonic Dismembrator Model 500, Fisher, Max Output 400W. 70% power, 8 × 10 s bursts with 30 s pauses). The lysate was cleared by centrifugation (30 min, 20,000 rpm, 4°C) and purified over Ni-NTA beads (Qiagen) onto a gravity flow column. After the resin was extensively washed in PBS, supplemented with 7mM βME and 20mM imidazole, the protein was eluted with the wash buffer containing 500mM imidazole. The eIF4E protein was then dialyzed overnight against PBS buffer containing 1mM DTT in the presence of the TEV protease. High level of purity (>95%) was further achieved by gel filtration on Superdex 200pg column (GE-Biosciences) in 50mM Sodium phosphate (pH 7.2), 100mM NaCl, 1mM DTT.

In addition to the above purification in native conditions, eIF4E was also purified in denaturing conditions using the pellet resulting from the lysate clarification. The pellet was resuspended in 50mM Tris pH 7.5, 6M Guanidine-HCl, 7mM βME, 10mM imidazole and lysed by sonication (same protocol as used for native eIF4E). After incubation with end-over-end rotation at room temperature for 30 min, the cleared lysate was incubated with Ni-NTA agarose resin in batches for 1h. The Ni-agarose resin was washed with 50mM Hepes pH 7.5, 6M Guanidine-HCl, 7mM βME, 20mM imidazole, and the unfolded eIF4E was eluted in 3ml of the wash buffer containing 500mM imidazole. The protein was quickly refolded by diluting it drop by drop into cold buffer containing 50mM Hepes pH 7.5, 200mM NaCl, 1mM DTT, 1M 3-(1-Pyridinio)-1-propanesulfonate (NDSB201). The final eIF4E concentration was kept lower than 0.1mg/ml. After mixing for 1h at 4°C, the refolded protein was concentrated and dialyzed against PBS, 1mM DTT. As above, the tags were removed by the TEV protease and eIF4E was subjected to gel filtration. Importantly, the ^{15}N- and ^{13}C-HSQCs for eIF4E purified in both native and denaturing conditions were similar.

The ILV methyl labelled eIF4E was prepared from cells grown on minimal M9 media containing 2g/L [^{15}N]ammonium chloride and 2g/L [$^{13}C_6$, ^{2}H]glucose (Sigma-Aldrich). *E. coli* strains were adapted to deuterated minimal medium by gradually increasing the deuterium content. Briefly, freshly transformed colonies were used to start a 25ml culture in LB medium/H_2O, followed by successive pre-cultures in M9 media containing 0%, 50% and 100% D_2O. Each pre-culture was initiated to an OD600 of 0.25. In the final culture, the ^{13}C-labeled precursors α-ketoisovalerate and α-ketobutyrate (Sigma-Alrich) were added 1h before induction at 100 mg/L and 60 mg/L, respectively.

Full-length human RNMT was expressed in pGEX-6p1 plasmid, while RNMT Δ1–163 (RNMT-C) and RNMT Δ1–163 Δ417–456 (RNMT-C Δlobe) were inserted into the pET-28a vector between the BamHI and XhoI restriction sites, in which a TEV protease cleavage site was inserted between the T7 tag and RNMT leaving the sequence Gly-Cys attached to the N-terminus of the protein. Plasmids were overexpressed in *Escherichia coli* BL21(DE3) cells in the NZY auto-induction LB medium (*nzytech*) at 37°C and induced overnight at 20°C. Cells were harvested by centrifugation and stored at −20°C until use. Full-length RNMT was purified as described in [24]. For truncated RNMT in pET-28a plasmid (wild type and mutants), the frozen cells were resuspended in 50mM Hepes pH 7.5 supplemented with 500mM NaCl, 5% glycerol, 7mM β-mercaptoethanol (βME), 1mg/ml lysozyme, cocktail of protease inhibitor (GE), 10mM imidazole, and lysed by sonication on ice (Sonic Dismembrator Model 500, Fisher, Max Output 400W. 70% power, 8–12 × 10 s bursts with 30 s pauses). The lysate was cleared by centrifugation (30 min, 20,000 rpm, 4°C) and purified over Ni-NTA beads (Qiagen) onto a gravity flow column. After the resin was extensively washed using 20mM Hepes pH 7.5, 500mM NaCl, 5% glycerol, 7mM βME, 20mM imidazole, the protein was eluted with the wash buffer containing 500mM imidazole. The RNMT protein was then dialyzed overnight against 20mM Hepes pH 7.5, 200mM NaCl, 7mM βME in the presence of the TEV protease. High level of purity (>95%) was further achieved by size exclusion chromatography on Superdex 200pg column (GE-Biosciences) in 50mM Sodium phosphate (pH 7.2), 100mM NaCl, 1mM DTT.

The RNMT-C/RAM complex was purified as follow: half a liter of GST-RAM was first overexpressed in BL21(DE3) and purified over glutathione Sepharose 4B beads (GE Healthcare) onto a gravity flow column[24]. After the beads were washed, lysate from 1 liter of His-tagged RNMT-C was added to the resin containing the GST-RAM and mixed by rotation for 1h. After the resin was washed, the GST-RAM/HIS-RNMT-C was eluted with the wash buffer containing 50mM reduced glutathione. The complex was dialyzed overnight against 20mM Hepes pH 7.5, 200mM NaCl, 7mM βME in the presence of the TEV protease (to cleave the His-tag from RNMT) and the prescission protease (to cleave the GST-tag from RAM). The complex was further purified by size exclusion chromatography on a Superdex 200pg column (GE-Biosciences) in 50mM Sodium phosphate (pH 7.2), 100mM NaCl, 1mM DTT.

Full-length human 4E-BP1 and 4E-BP2 were expressed in pET-15b plasmids. Both plasmids were overexpressed in *Escherichia coli* BL21(DE3) cells in LB rich medium at 37°C and induced overnight by 0.5 mM IPTG at 30°C. Cells were harvested by centrifugation and stored at −20°C until use. The frozen cells were resuspended in 2x PBS supplemented with 0.5% IGEPAL, 5mM βME, 1mg/ml lysozyme, cocktail of protease inhibitor (GE), 10mM imidazole, and lysed by sonication (Sonic Dismembrator Model 500, Fisher, Max Output 400W. 60% power, 7 × 10 s bursts with 30 s pauses). The lysate was cleared by centrifugation (30 min, 20,000 rpm, 4°C) and purified over Ni-NTA beads (Qiagen) onto a gravity flow column. After the resin was extensively washed using PBS, 5mM βME, 20mM imidazole, the protein was eluted with the wash buffer containing 500mM imidazole. 4E-BP proteins were then dialyzed overnight against PBS and 1mM DTT in the presence of the thrombin protease. High level of purity (>95%) was further achieved by gel filtration on Superdex 75pg column (GE-Biosciences) in 50mM Sodium phosphate (pH 7.2), 100mM NaCl, 1mM DTT. Full-length LRPPRC was purified as described in [52].

The eIF4GI peptide, 4Gp, (fragment 621–637, sequence KKQYDREFLLDFQFMPA) was synthesized by fluorenylmethoxycarbonyl (Fmoc) solid-phase peptide synthesis and purified by reverse phase chromatography on a C18 Vydac column. The composition and purity of the peptide was verified by ion-spray quadrupole mass spectroscopy.

Protein Pull-downs

GST and GST-eIF4E proteins were immobilized on glutathione Sepharose 4B (GE Healthcare) at 10 pmol of protein per microliter of beads in PBS supplemented with 1 mM DTT. For each binding reaction, 10 μl of GST or GST-eIF4E was incubated with 20 pmol of RNMT (wild-type or mutants) in 350 μl of binding buffer (20 mM Hepes pH 7.5, 110 mM potassium acetate, 2 mM magnesium acetate, 0.3% Igepal, 1 mM EGTA, 20 mM DTT) and mixed by rotation for 2 h at 4°C. Unbound protein was removed by washing five times with binding buffer, and bound proteins were eluted with hot Laemmli sample buffer. The eluted protein complexes were then separated by SDS/PAGE and western blotting. In additional competition experiments, the eIF4GI peptide (4Gp), the full-length 4E-BP1 and 4E-BP2 (at a 5-fold molar excess with GST-eIF4E) or m^7GDP (20-fold molar excess) were added and left for equilibration with the GST-eIF4E at room temperature for 15min before adding the appropriate RNMT constructs and the binding buffer. We note that because RNMT-C

migrates between GST and GST-eIF4E we used the same samples but ran these on separate gels. One gel was reserved for GST proteins and other gels for proteins that were in this overlapping range.

m^7GTP-Agarose Affinity Chromatography

Cap affinity chromatography was carried out as described in [57]. Briefly, twenty microliters of m^7GTP-Agarose bead slurry (γ-Aminophenyl-m^7GTP (C10-spacer)-Agarose, Jena Bioscience, Catalog No. AC-155S) was washed three times with 1.5 mL buffer B (0.1M sodium phosphate, Biobasic), 0.3M NaCl (Fisher Chemical), 10μM protease-free BSA (Catalog No. BP9703–100), 0.1% IGEPAL (Catalog No. 198596, pH 7.5). Beads were bound separately with 2μM 4E or 400 nM RNMT in buffer B for 30 min at room temperature with rotation at low speed (16 rpm). Unbound proteins were removed from beads by washing three times with 1.5 mL Buffer B. Bound eIF4E was incubated separately with RNMT (400 nM), GDP (50 μM), or m^7GTP (50 μM) in Buffer B for 30 min at room temperature with rotation at low speed (16 rpm). Beads were washed three times with Buffer B. All centrifugation during washing steps were done at 500xg. Bound proteins were eluted from m^7GTP-Agarose beads by boiling in 50 μL of Laemmli buffer. After brief centrifugation at high speed (room temperature, 16000 ×g), supernatants were isolated and eluted proteins were resolved on SDS/PAGE and visualized by Western blotting.

Antibodies used in Western Blots

Primary antibodies mouse RNMT (RNMT 3H3–1D12, Santa Cruz Biotechnology, Catalog No. sc-517112) and mouse eIF4E (BD Biosciences, 610269), rabbit polyclonal RNMT (ProteinTech, 13743–1-AP), rabbit monoclonal 4E-BP1 (53H11, Cell Signaling Technology, #9644), rabbit polyclonal 4E-BP2, Cell Signaling Technology #2845, rabbit polyclonal RAM (FAM103A1 Polyclonal antibody, ProteinTech, 19422–1-AP) and GST Goat Polyclonal (Cytiva; catalog no. 45-001-369).

Methyl transferase assay

N-7 cap guanosine methylation assay was performed according to[34]. Briefly, 20 μM recombinant human RNMT 167–476 mixed with 0, 10, 20 80 μM recombinant human eIF4E and an *in vitro* transcribed 55-nt ^{32}P-capped RNA and 200 nM s-adenosyl methionine for 10 min at 30°C. RNA was purified and digested with P1 nuclease and cap structures resolved on PEI cellulose in 0.4 M ammonium sulphate.

NMR studies

NMR experiments were recorded at 600 MHz on a Bruker Avance III HD spectrometer equipped with a QCIP cryoprobe at 20°C unless otherwise stated. Experiments to extend the number the backbone ^{15}N/^{13}C assignments eIF4E in apo and cap bound forms were performed on the ILV labeled sample. 3D HNCA, HNCACB and CBCA(CO)NH experiments were ran in a non-uniform manner using the Bruker standard parameter sequences with 15 to 20% Poisson Gap Sampling Schemes [58]. ILV methyl side-chain chemical shift assignments were obtained from the out-and-back ^{13}C-^{13}C TOCSY experiment ((H)C-TOCSY-S-TOCSY-(C)H) [59] in 100% D_2O (τ_m = 14.13 ms). Non

uniform acquisition and processing were performed as described [59]. A ^{13}C-^{13}C NOESY was also measured with a mixing time of 120 ms [60]. Assignments have been deposited in the BMRB database with accession No. 27427 for the apo-eIF4E and 27428 for the m^7GDP-bound eIF4E.Non-uniform sampling spectra were processed using SMILE [61] and NMRPipe [62]. Uniformly acquired data were processed with NMR pipe,: spectra were analyzed with Sparky [63] or NMRViewJ[64]. ^{1}H-^{15}N HSQC spectra to determine binding of eIF4E and RNMT were ran using the BEST sequence [65] with 50 μM ^{15}N labelled eIF4E in the absence and presence of 200 μM unlabelled RNMT (RNMT-FL, RNMT-C and RNMT-C Δlobe) in 50 mM sodium phosphate,100 mM NaCl, 1 mM DTT, 7% D_2O, pH 7.2. Spectra were analysed using NMRViewJ with the ratios calculated from peak heights of eIF4E in the absence and presence of the various RNMT constructs. Values for the diameter of methyl groups (yellow balls) in Figure 2G,H were calculated with the following equation: $d = - (rat - 0.89) / 0.17$ where d is the diameter and rat is the ratio of peak intensities between the complex and free eIF4E. The graphic representations of the 3D structures were rendered using PyMOL (The PyMOL Molecular Graphics System, Version 1.7.4 Schrödinger, LLC) and Molmol [66].

TCS experiments [47] were acquired at 20°C on 150 μM [U-^{2}H-^{15}N] eIF4E with 2.4mM m^7GDP in the presence and absence of 110 μM unlabelled RNMT-C. Experiments were also ran with 110 μM eIF4E and 37.5 μM in the absence of m^7GDP. On and off-resonance experiments were acquired in an interleaved manner, with a train of REBURP pulses exciting 1000 Hz at −0.5ppm and −40 ppm, respectively. A predominately deuterated buffer (30%H_2O/70%D_2O) of 50 mM phosphate, 150 mM NaCl, 1mM DTT, 0.02% NaN_3 was used to minimise the effects of spin diffusion. Spectra were processed with NMRPipe and analysed with NMRView. Due to the presence of high proton content in the eIF4E sample, the data were analysed by comparing the changes in the intensities for eIF4E NH peaks with (I_{on}) and without (I_{off}) saturation in the presence and absence of RNMT-C [49]. Values below the mean line exhibit stronger cross saturation, values above, are not physically possible and may reflect degradation of the sample(s) over time. Using a cutoff of the mean change ± 0.66*SD (bottom and top lines (Figure 2C))[51] reveals that the only outliers observed have stronger cross saturation in the complex.

Circular dichroism spectroscopy

Far-UV CD spectra were collected using Jasco-810 spectropolarimeter with 0.2 cm cuvette at room temperature. The solution conditions were 20 mM phosphate buffer (pH 7.2), 50 mM NaCl, 1 mM DTT. All of the measurements were repeated two times with a 1 nm bandwidth. Relative ellipticity was converted to mean residue molar ellipticity according to [67]. HT voltage for data shown was below 600. Contributions from the buffer alone were subtracted.

Haddock-derived structure of the eIF4E-RNMT-C complex

The Haddock2.4 webserver [51] was used to generate restraint-driven docking for interaction between eIF4E and RNMT-C using the standard protocols with the coordinates of eIF4E (PDB ID code 2GPQ) and RNMT (PDB ID code 5E8J). The following residues were selected for the active ambiguous interaction restraints (AIRs) as input to Haddock:

residues 294, 374 and 380 of RNMT chosen based on the mutational and pull-down data and 7 residues of eIF4E based on TCS and ^{13}C chemical shift broadening (69, 70, 73, 75, 77, 182, 187). Default Haddock settings were used for the docking, generating a final 200 structures. The final models were clustered based on the fraction of common contacts using a 0.60 cutoff. Electrostatic potentials were calculated via the APBS (Adaptive Poisson-Boltzmann Solver) software [68]

Cross-linking Mass spectrometry

Cross-linking of recombinant protein heterodimers, heterodimers enrichment, mass spectrometry and subsequent data analysis were carried out as previously described in [45] except for the following minor changes. Proteins were cross-linked with DSS for 30 minutes, and heterodimer fractions enriched on Superdex-75 column 10/300 GL were directly digested with MS grade Trypsin/LysC Mix (Promega) overnight in a 1:20 enzyme to protein ratio. Multiply charged peptide were enriched on MCX as previously described [45] or on μZipTips (EMD Millipore). Peptides were eluted from the LC-MS column at a flow rate of 250 nl min^{-1} using a 3-slope gradient of 0.2 % formic acid (FA) in water (buffer A) and 0.2 % FA in 100 % acetonitrile (buffer B). For all samples, concentration of buffer B first increased from 2 % to 15 % over 6 min. The second gradient slopes varied depending on sample acquisition dates and sample processing. For the first sample set, solution B was increased from 15 % to 50 % over 45 min for all samples. For the second sample set, buffer B was increased to 50 % over 34 min for MCX cleaned samples, while the same % of solution B was achieved over 39 min for peptides cleaned on μZipTips (EMD Millipore). The third slope was identical for all samples, in which solution B increased from 50 % to 85% over 5 min. Data analysis was carried out using Sim-XL v1.5.5.2 [69, 70] with trypsin and LysC indicated as cleaving proteases.

Supplementary Material

Refer to Web version on PubMed Central for supplementary material.

Acknowledgements.

KLBB acknowledges funding from NIH RO1 80728, NIH RO1 98571, and holds a Canada Research Chair in Molecular Biology of the Cell Nucleus. The content is solely the responsibility of the authors and does not necessarily represent the official views of the National Institutes of Health. VHC holds an MRC Senior Fellowship.

References

[1]. Furuichi Y Discovery of m(7)G-cap in eukaryotic mRNAs. Proc Jpn Acad Ser B Phys Biol Sci 2015;91:394–409.

[2]. Cowling VH. Regulation of mRNA cap methylation. The Biochemical journal. 2010;425:295–302.

[3]. Galloway A, Cowling VH. mRNA cap regulation in mammalian cell function and fate. Biochim Biophys Acta Gene Regul Mech 2019;1862:270–9. [PubMed: 30312682]

[4]. Borden K, Culjkovic-Kraljacic B, Cowling VH. To cap it all off, again: dynamic capping and recapping of coding and non-coding RNAs to control transcript fate and biological activity. Cell Cycle. 2021;20:1347–60. [PubMed: 34241559]

[5]. Culjkovic-Kraljacic B, Skrabanek L, Revuelta MV, Gasiorek J, Cowling VH, Cerchietti L, et al. The eukaryotic translation initiation factor eIF4E elevates steady-state m(7)G capping of coding and noncoding transcripts. Proc Natl Acad Sci U S A. 2020;117:26773–83. [PubMed: 33055213]

[6]. Schoenberg DR, Maquat LE. Re-capping the message. Trends in biochemical sciences. 2009;34:435–42. [PubMed: 19729311]

[7]. Jiao X, Xiang S, Oh C, Martin CE, Tong L, Kiledjian M. Identification of a quality-control mechanism for mRNA 5'-end capping. Nature. 2010;467:608–11. [PubMed: 20802481]

[8]. Otsuka Y, Kedersha NL, Schoenberg DR. Identification of a cytoplasmic complex that adds a cap onto 5'-monophosphate RNA. Molecular and cellular biology. 2009;29:2155–67. [PubMed: 19223470]

[9]. Jiao Y, Riechmann JL, Meyerowitz EM. Transcriptome-wide analysis of uncapped mRNAs in Arabidopsis reveals regulation of mRNA degradation. Plant Cell. 2008;20:2571–85. [PubMed: 18952771]

[10]. Lim SK, Maquat LE. Human beta-globin mRNAs that harbor a nonsense codon are degraded in murine erythroid tissues to intermediates lacking regions of exon I or exons I and II that have a cap-like structure at the 5' termini. EMBO J 1992;11:3271–8. [PubMed: 1324170]

[11]. Cowling VH, Cole MD. The Myc transactivation domain promotes global phosphorylation of the RNA polymerase II carboxy-terminal domain independently of direct DNA binding. Molecular and cellular biology. 2007;27:2059–73. [PubMed: 17242204]

[12]. Cowling VH. Myc up-regulates formation of the mRNA methyl cap. Biochemical Society transactions. 2010;38:1598–601. [PubMed: 21118133]

[13]. Grasso L, Suska O, Davidson L, Gonatopoulos-Pournatzis T, Williamson R, Wasmus L, et al. mRNA Cap Methylation in Pluripotency and Differentiation. Cell Rep 2016;16:1352–65. [PubMed: 27452456]

[14]. Aregger M, Kaskar A, Varshney D, Fernandez-Sanchez ME, Inesta-Vaquera FA, Weidlich S, et al. CDK1-Cyclin B1 Activates RNMT, Coordinating mRNA Cap Methylation with G1 Phase Transcription. Mol Cell. 2016;61:734–46. [PubMed: 26942677]

[15]. Mukherjee C, Patil DP, Kennedy BA, Bakthavachalu B, Bundschuh R, Schoenberg DR. Identification of cytoplasmic capping targets reveals a role for cap homeostasis in translation and mRNA stability. Cell Rep 2012;2:674–84. [PubMed: 22921400]

[16]. Mao X, Schwer B, Shuman S. Yeast mRNA cap methyltransferase is a 50-kilodalton protein encoded by an essential gene. Molecular and cellular biology. 1995;15:4167–74. [PubMed: 7623811]

[17]. Chu C, Shatkin AJ. Apoptosis and autophagy induction in mammalian cells by small interfering RNA knockdown of mRNA capping enzymes. Molecular and cellular biology. 2008;28:5829–36. [PubMed: 18678651]

[18]. Pillutla RC, Shimamoto A, Furuichi Y, Shatkin AJ. Human mRNA capping enzyme (RNGTT) and cap methyltransferase (RNMT) map to 6q16 and 18p11.22-p11.23, respectively. Genomics. 1998;54:351–3. [PubMed: 9828141]

[19]. Shafer B, Chu C, Shatkin AJ. Human mRNA cap methyltransferase: alternative nuclear localization signal motifs ensure nuclear localization required for viability. Molecular and cellular biology. 2005;25:2644–9. [PubMed: 15767670]

[20]. Srinivasan P, Piano F, Shatkin AJ. mRNA capping enzyme requirement for Caenorhabditis elegans viability. The Journal of biological chemistry. 2003;278:14168–73. [PubMed: 12576475]

[21]. Tsukamoto T, Shibagaki Y, Murakoshi T, Suzuki M, Nakamura A, Gotoh H, et al. Cloning and characterization of two human cDNAs encoding the mRNA capping enzyme. Biochem Biophys Res Commun 1998;243:101–8. [PubMed: 9473487]

[22]. Yamada-Okabe T, Doi R, Shimmi O, Arisawa M, Yamada-Okabe H. Isolation and characterization of a human cDNA for mRNA 5'-capping enzyme. Nucleic Acids Res 1998;26:1700–6. [PubMed: 9512541]

[23]. Yue Z, Maldonado E, Pillutla R, Cho H, Reinberg D, Shatkin AJ. Mammalian capping enzyme complements mutant Saccharomyces cerevisiae lacking mRNA guanylyltransferase and selectively binds the elongating form of RNA polymerase II. Proc Natl Acad Sci U S A. 1997;94:12898–903. [PubMed: 9371772]

[24]. Gonatopoulos-Pournatzis T, Dunn S, Bounds R, Cowling VH. RAM/Fam103a1 is required for mRNA cap methylation. Mol Cell. 2011;44:585–96. [PubMed: 22099306]

[25]. Fabrega C, Hausmann S, Shen V, Shuman S, Lima CD. Structure and mechanism of mRNA cap (guanine-N7) methyltransferase. Mol Cell. 2004;13:77–89. [PubMed: 14731396]

[26]. Varshney D, Lombardi O, Schweikert G, Dunn S, Suska O, Cowling VH. mRNA Cap Methyltransferase, RNMT-RAM, Promotes RNA Pol II-Dependent Transcription. Cell Rep 2018;23:1530–42. [PubMed: 29719263]

[27]. Trotman JB, Giltmier AJ, Mukherjee C, Schoenberg DR. RNA guanine-7 methyltransferase catalyzes the methylation of cytoplasmically recapped RNAs. Nucleic Acids Res 2017;45:10726–39. [PubMed: 28981715]

[28]. Boutz PL, Bhutkar A, Sharp PA. Detained introns are a novel, widespread class of post-transcriptionally spliced introns. Genes Dev 2015;29:63–80. [PubMed: 25561496]

[29]. Girard C, Will CL, Peng J, Makarov EM, Kastner B, Lemm I, et al. Post-transcriptional spliceosomes are retained in nuclear speckles until splicing completion. Nat Commun 2012;3:994. [PubMed: 22871813]

[30]. Prasanth KV, Prasanth SG, Xuan Z, Hearn S, Freier SM, Bennett CF, et al. Regulating gene expression through RNA nuclear retention. Cell. 2005;123:249–63. [PubMed: 16239143]

[31]. Culjkovic B, Borden KL. Understanding and Targeting the Eukaryotic Translation Initiation Factor eIF4E in Head and Neck Cancer. J Oncol 2009;2009:981679. [PubMed: 20049173]

[32]. Volpon L, Osborne MJ, Borden KLB. Biochemical and Structural Insights into the Eukaryotic Translation Initiation Factor eIF4E. Curr Protein Pept Sci 2019;20:525–35. [PubMed: 30636602]

[33]. Borden KLB, Volpon L. The diversity, plasticity, and adaptability of cap-dependent translation initiation and the associated machinery. RNA Biol 2020;17:1239–51. [PubMed: 32496897]

[34]. Varshney D, Petit AP, Bueren-Calabuig JA, Jansen C, Fletcher DA, Peggie M, et al. Molecular basis of RNA guanine-7 methyltransferase (RNMT) activation by RAM. Nucleic Acids Res 2016;44:10423–36. [PubMed: 27422871]

[35]. Wen Y, Shatkin AJ. Cap methyltransferase selective binding and methylation of GpppG-RNA are stimulated by importin-alpha. Genes Dev 2000;14:2944–9. [PubMed: 11114884]

[36]. Culjkovic-Kraljacic B, Fernando TM, Marullo R, Calvo-Vidal N, Verma A, Yang S, et al. Combinatorial targeting of nuclear export and translation of RNA inhibits aggressive B-cell lymphomas. Blood. 2016;127:858–68. [PubMed: 26603836]

[37]. Culjkovic B, Topisirovic I, Skrabanek L, Ruiz-Gutierrez M, Borden KL. eIF4E promotes nuclear export of cyclin D1 mRNAs via an element in the 3'UTR. J Cell Biol 2005;169:245–56. [PubMed: 15837800]

[38]. Culjkovic B, Topisirovic I, Skrabanek L, Ruiz-Gutierrez M, Borden KL. eIF4E is a central node of an RNA regulon that governs cellular proliferation. J Cell Biol 2006;175:415–26. [PubMed: 17074885]

[39]. Topisirovic I, Siddiqui N, Lapointe VL, Trost M, Thibault P, Bangeranye C, et al. Molecular dissection of the eukaryotic initiation factor 4E (eIF4E) export-competent RNP. EMBO J 2009;28:1087–98. [PubMed: 19262567]

[40]. Topisirovic I, Guzman ML, McConnell MJ, Licht JD, Culjkovic B, Neering SJ, et al. Aberrant eukaryotic translation initiation factor 4E-dependent mRNA transport impedes hematopoietic differentiation and contributes to leukemogenesis. Molecular and cellular biology. 2003;23:8992–9002. [PubMed: 14645512]

[41]. Cohen N, Sharma M, Kentsis A, Perez JM, Strudwick S, Borden KL. PML RING suppresses oncogenic transformation by reducing the affinity of eIF4E for mRNA. Embo J 2001;20:4547–59. [PubMed: 11500381]

[42]. Topisirovic I, Culjkovic B, Cohen N, Perez JM, Skrabanek L, Borden KL. The proline-rich homeodomain protein, PRH, is a tissue-specific inhibitor of eIF4E-dependent cyclin D1 mRNA transport and growth. Embo J 2003;22:689–703. [PubMed: 12554669]

[43]. Rong L, Livingstone M, Sukarieh R, Petroulakis E, Gingras AC, Crosby K, et al. Control of eIF4E cellular localization by eIF4E-binding proteins, 4E-BPs. RNA. 2008;14:1318–27. [PubMed: 18515545]

[44]. Aregger M, Cowling VH. Human cap methyltransferase (RNMT) N-terminal non-catalytic domain mediates recruitment to transcription initiation sites. The Biochemical journal. 2013;455:67–73. [PubMed: 23863084]

[45]. Coutinho de Oliveira L, Volpon L, Rahardjo AK, Osborne MJ, Culjkovic-Kraljacic B, Trahan C, et al. Structural studies of the eIF4E-VPg complex reveal a direct competition for capped RNA: Implications for translation. Proc Natl Acad Sci U S A. 2019;116:24056–65. [PubMed: 31712417]

[46]. Volpon L, Culjkovic-Kraljacic B, Osborne MJ, Ramteke A, Sun Q, Niesman A, et al. Importin 8 mediates m7G cap-sensitive nuclear import of the eukaryotic translation initiation factor eIF4E. Proc Natl Acad Sci U S A. 2016;113:5263–8. [PubMed: 27114554]

[47]. Nakanishi T, Miyazawa M, Sakakura M, Terasawa H, Takahashi H, Shimada I. Determination of the interface of a large protein complex by transferred cross-saturation measurements. Journal of molecular biology. 2002;318:245–9. [PubMed: 12051834]

[48]. Volpon L, Osborne MJ, Topisirovic I, Siddiqui N, Borden KL. Cap-free structure of eIF4E suggests a basis for conformational regulation by its ligands. EMBO J 2006;25:5138–49. [PubMed: 17036047]

[49]. Deep S, Im SC, Zuiderweg ER, Waskell L. Characterization and calculation of a cytochrome c-cytochrome b5 complex using NMR data. Biochemistry. 2005;44:10654–68. [PubMed: 16060674]

[50]. Sprangers R, Velyvis A, Kay LE. Solution NMR of supramolecular complexes: providing new insights into function. Nat Methods. 2007;4:697–703. [PubMed: 17762877]

[51]. van Zundert GC, Bonvin AM. Modeling protein-protein complexes using the HADDOCK webserver “modeling protein complexes with HADDOCK”. Methods Mol Biol 2014;1137:163–79. [PubMed: 24573481]

[52]. Volpon L, Culjkovic-Kraljacic B, Sohn HS, Blanchet-Cohen A, Osborne MJ, Borden KLB. A biochemical framework for eIF4E-dependent mRNA export and nuclear recycling of the export machinery. RNA. 2017;23:927–37. [PubMed: 28325843]

[53]. Bah A, Vernon RM, Siddiqui Z, Krzeminski M, Muhandiram R, Zhao C, et al. Folding of an intrinsically disordered protein by phosphorylation as a regulatory switch. Nature. 2015;519:106–9. [PubMed: 25533957]

[54]. Siddiqui N, Tempel W, Nedyalkova L, Volpon L, Wernimont AK, Osborne MJ, et al. Structural insights into the allosteric effects of 4EBP1 on the eukaryotic translation initiation factor eIF4E. Journal of molecular biology. 2012;415:781–92. [PubMed: 22178476]

[55]. Ptushkina M, von der Haar T, Vasilescu S, Frank R, Birkenhager R, McCarthy JE. Cooperative modulation by eIF4G of eIF4E-binding to the mRNA 5’ cap in yeast involves a site partially shared by p20. Embo J 1998;17:4798–808. [PubMed: 9707439]

[56]. Sung H, Kang SH, Bae YJ, Hong JT, Chung YB, Lee CK, et al. PCR-based detection of Mycoplasma species. J Microbiol 2006;44:42–9. [PubMed: 16554716]

[57]. Kentsis A, Topisirovic I, Culjkovic B, Shao L, Borden KL. Ribavirin suppresses eIF4E-mediated oncogenic transformation by physical mimicry of the 7-methyl guanosine mRNA cap. Proc Natl Acad Sci U S A. 2004;101:18105–10. [PubMed: 15601771]

[58]. Hyberts SG, Takeuchi K, Wagner G. Poisson-gap sampling and forward maximum entropy reconstruction for enhancing the resolution and sensitivity of protein NMR data. J Am Chem Soc 2010;132:2145–7. [PubMed: 20121194]

[59]. Kerfah R, Hamelin O, Boisbouvier J, Marion D. CH3-specific NMR assignment of alanine, isoleucine, leucine and valine methyl groups in high molecular weight proteins using a single sample. J Biomol NMR. 2015;63:389–402. [PubMed: 26566791]

[60]. Bermel W, Bertini I, Felli IC, Kummerle R, Pierattelli R. 13C direct detection experiments on the paramagnetic oxidized monomeric copper, zinc superoxide dismutase. J Am Chem Soc 2003;125:16423–9. [PubMed: 14692785]

[61]. Ying J, Delaglio F, Torchia DA, Bax A. Sparse multidimensional iterative lineshape-enhanced (SMILE) reconstruction of both non-uniformly sampled and conventional NMR data. J Biomol NMR. 2017;68:101–18. [PubMed: 27866371]

[62]. Delaglio F, Grzesiek S, Vuister GW, Zhu G, Pfeifer J, Bax A. NMRPipe: a multidimensional spectral processing system based on UNIX pipes [see comments]. J Biomol NMR. 1995;6:277–93. [PubMed: 8520220]

[63]. Goddard TD, Kneller DG. Sparky 3, University of California, San Francisco, CA. 2003.

[64]. Johnson BA, Blevins RA. NMR View: A computer program for the visualization and analysis of NMR data. J Biomol NMR. 1994;4:603–14. [PubMed: 22911360]

[65]. Lescop E, Schanda P, Brutscher B. A set of BEST triple-resonance experiments for time-optimized protein resonance assignment. J Magn Reson 2007;187:163–9. [PubMed: 17468025]

[66]. Koradi R, Billeter M, Wuthrich K. MOLMOL: a program for display and analysis of macromolecular structures. J Mol Graph 1996;14:51–5, 29–32. [PubMed: 8744573]

[67]. Fasman GD. Circular dichroism and the conformational analysis of biomolecules. New York: Plenum Press; 1996.

[68]. Jurrus E, Engel D, Star K, Monson K, Brandi J, Felberg LE, et al. Improvements to the APBS biomolecular solvation software suite. Protein Sci 2018;27:112–28. [PubMed: 28836357]

[69]. Lima DB, Melchior JT, Morris J, Barbosa VC, Chamot-Rooke J, Fioramonte M, et al. Characterization of homodimer interfaces with cross-linking mass spectrometry and isotopically labeled proteins. Nat Protoc 2018;13:431–58. [PubMed: 29388937]

[70]. Lima DB, de Lima TB, Balbuena TS, Neves-Ferreira AGC, Barbosa VC, Gozzo FC, et al. SIM-XL: A powerful and user-friendly tool for peptide cross-linking analysis. J Proteomics. 2015;129:51–5. [PubMed: 25638023]

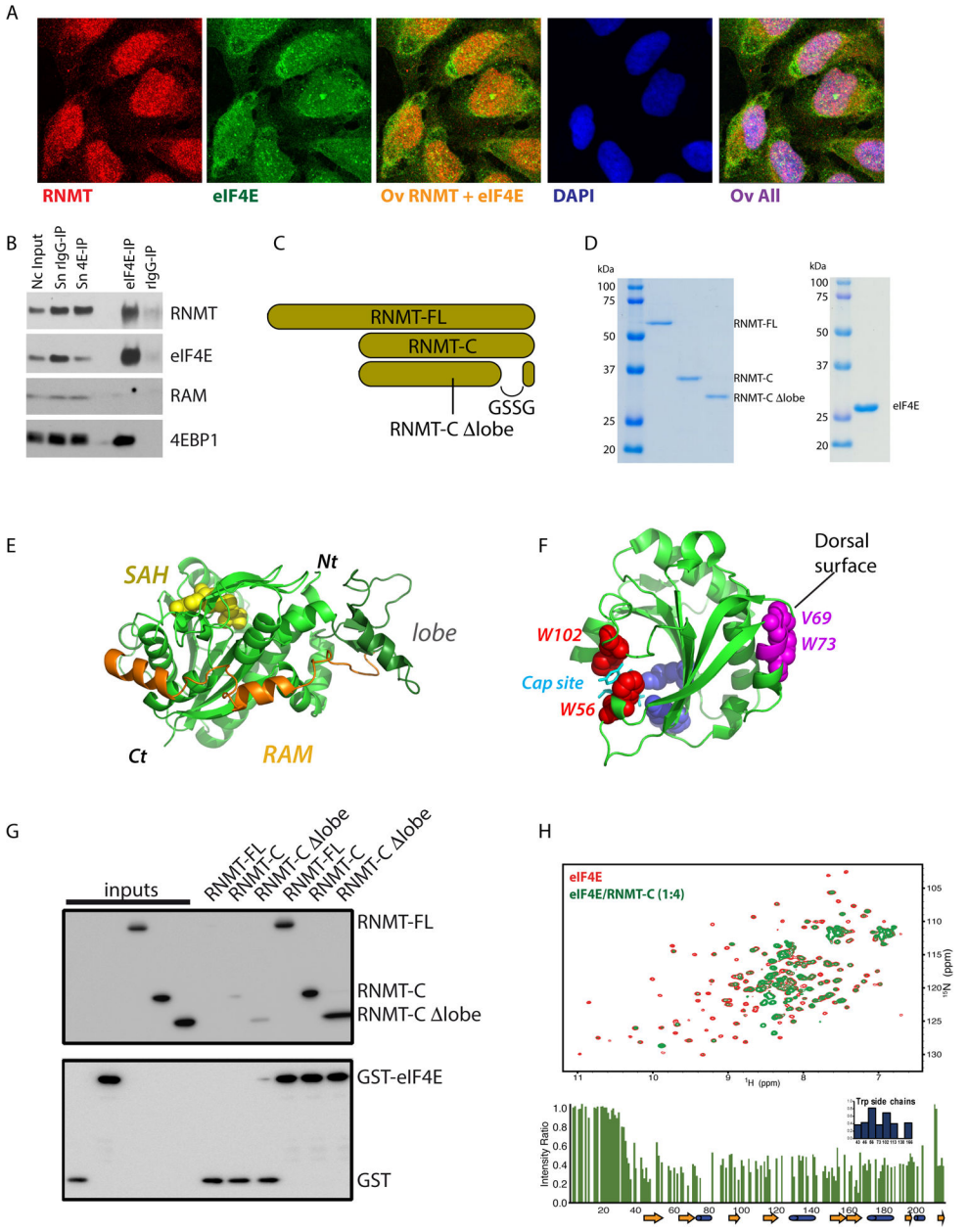

Figure 1. eIF4E and RNMT interact in vivo and in vitro.

A. Localization of RNMT and eIF4E in U2OS cells. Confocal micrographs of cells stained with anti-RNMT and anti-eIF4E antibodies and DAPI as a nuclear marker. Single and overlaid (Ov) channels are shown. Micrographs are single sections through the plane of the cells with 63x magnification. **B.** eIF4E and RNMT co-immunoprecipitated in the nuclear fractions of U2OS cells. Immunoprecipitations (IP) were carried out using U2OS nuclear lysates with rabbit anti-eIF4E (eIF4E-IP) or appropriate IgG control (rIgG-IP) and analyzed by Western blotting using antibodies as indicated. Nc indicates nuclear, Sn, supernatant. **C.** Schematic representation of the RNMT constructs used in this study: RNMT-FL (residues 1–476), RNMT-C (164–476) and RNMT-C Δlobe (RNMT-C with residues 416–456 replaced by a GSSG linker). **D.** SDS-PAGE gel of overexpressed and purified RNMT and eIF4E

constructs; molecular mass markers are shown. **E.** Crystal structure of RNMT-C (PDB 5E8J) in complex with RAM (orange) and SAH (yellow). The “lobe” region (dark green) is labelled. Nt indicates N-terminus and Ct, C-terminus. **F.** The two binding sites for eIF4E are shown on the crystal structure with m^7GTP (PDB 1L8B), the m^7GTP cap is shown as cyan sticks, W56 and W102 are shown as red spheres and blue spheres represent the charged basic residues (157,159 and 162). Residues critical for binding effector proteins at the dorsal surface (V69, W73) are shown in purple. **G.** GST or GST-eIF4E pulldown experiments for the following constructs, RNMT-FL, RNMT-C and RNMT-C Δlobe. **H.** Top, ^{1}H-^{15}N HSQC spectra of 50 μM ^{15}N-labelled eIF4E in the absence (red) and presence (green) 200 μM unlabelled RNMT-C. Bottom, per residue plot of the changes in peak intensity for backbone amides and side chain indole ^{15}NH resonances of ^{15}N labelled eIF4E upon addition of unlabelled RNMT-C shown in the top spectrum.

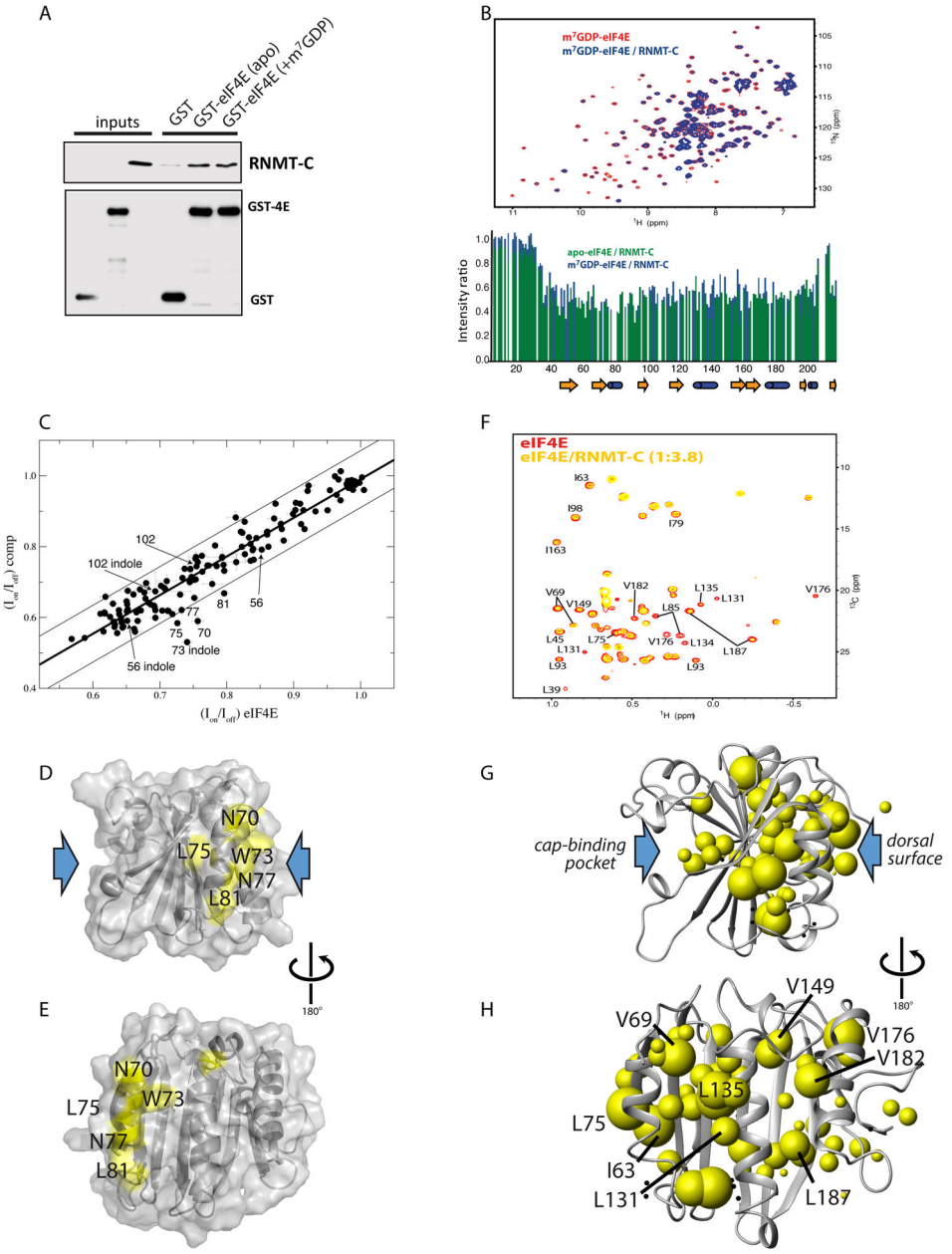

Figure 2. The cap-binding site of eIF4E is dispensable and the dorsal surface is employed by RNMT.

A. GST pulldown assay of GST-eIF4E for RNMT-C with and without incubation with m^7GDP reveals m^7GDP does not affect the eIF4E-RNMT-C interaction. **B.** Top, overlay of the ^{1}H-^{15}N HSQC spectra of m^7GDP cap (1mM) -bound ^{15}N eIF4E (50 μM) in the presence (blue) and absence (red) of 200 μM RNMT-C, indicating that in the presence of m^7GDP-cap the eIF4E-RNMT complex is still formed. Bottom, comparison of the changes in peak intensities for 50 μM ^{15}N eIF4E in the absence and presence of 200 μM RNMT-C (green bars) and m^7GDP cap (1 mM) bound ^{15}N eIF4E (50 μM) in the absence and presence of 200 μM RNMT-C (blue bar). Peaks were normalized to 1 for RNMT-C free complexes. **C.** Transferred cross saturation experiments. Intensity ratio (I_{on}/I_{off}) of RNMT-C complexed

eIF4E-m^{7}GDP amide ^{1}H resonances with (I_{on}) and without (I_{off}) saturation of aliphatic protons versus the same ratio in the absence of RNMT-C. Saturation was at −0.5ppm (1000 Hz bandwidth). The mean change is represented by the bold centre line, the top and bottom lines signify the mean value ± 0.66 standard deviation. **D,E** Location of residues identified from TCS experiments are mapped onto the surface of eIF4E (PDB, 2GPQ) and identify residues at the dorsal surface to be important in the RNMT interaction. **F.** ^{1}H-^{13}C HSQC spectrum of ILV-labelled eIF4E (50 μM) in the absence (red) and presence of RNMT-C (3.8 fold molar excess), yellow. **G,H.** Summary of the changes in intensity of ILV-labelled eIF4E methyl peaks induced by RNMT-C is mapped onto the structure of eIF4E, larger spheres represent larger broadening affects (see methods for details).

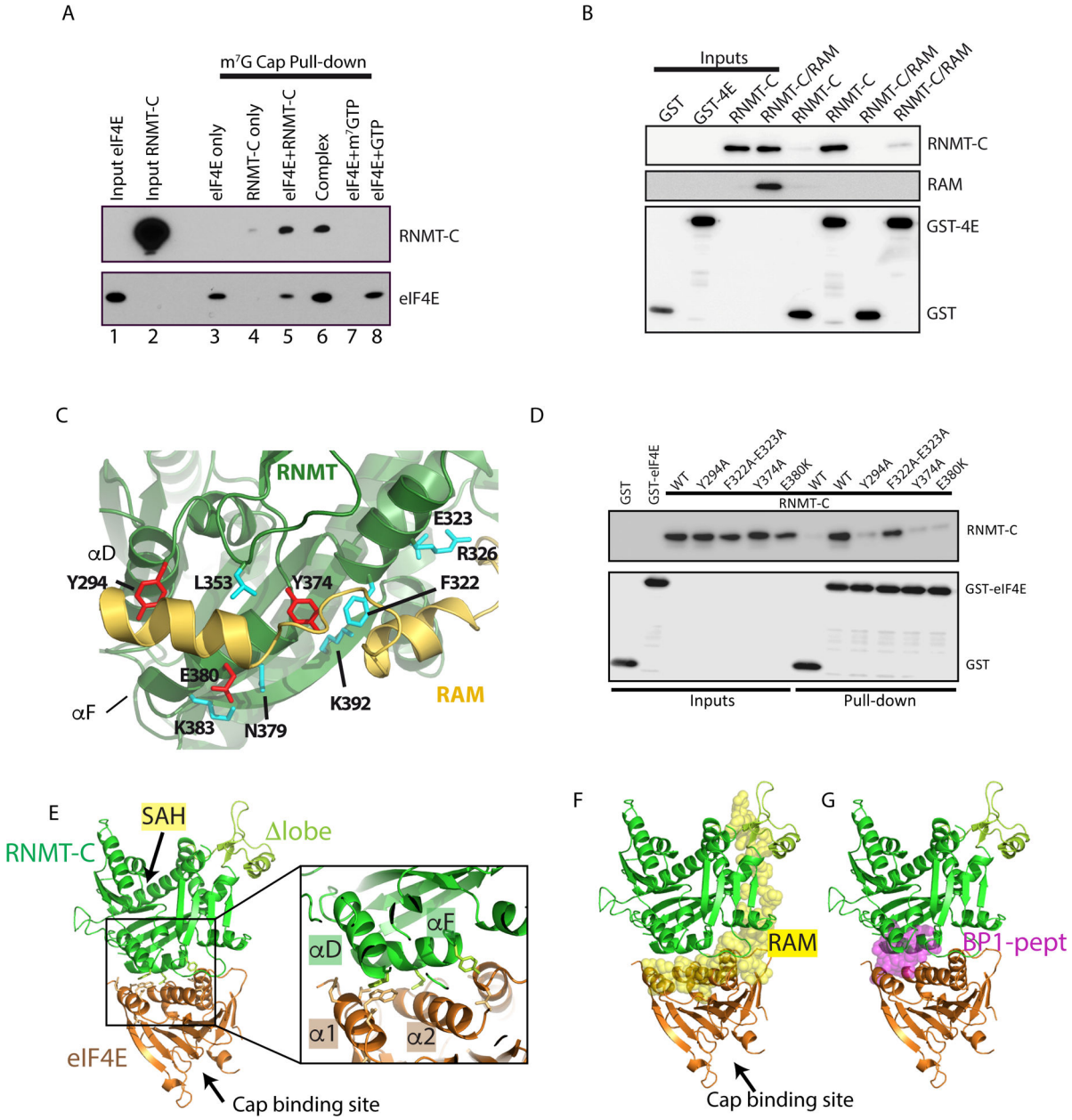

Figure 3. Identification of eIF4E-RNMT complex binding sites and structural models.

A. m^7GTP cap column chromatography for eIF4E in the presence or absence of RNMT-C. m^7GTP cap-bound proteins were analysed using Western blotting. m^7GTP-bound eIF4E binds to RNMT-C (lane 5, eIF4E protein was first bound to the m^7GTP column, and subsequently incubated with RNMT-C); eIF4E/RNMT-C complex binds to m^7GTP cap beads (labelled “complex” in lane 6, eIF4E was first incubated with RNMT-C to form a complex, and then incubated with m^7GTP beads). RNMT-C does not bind directly to m^7GTP beads (lane 4). 50μM m^7GTP elutes eIF4E from the m^7GTP beads (lane 7) while non-methylated GTP did not affect eIF4E binding to m^7GTP beads (lane 8), confirming specificity. Two percent input was used for eIF4E and RNMT-C. **B.** GST-eIF4E pulldown assays for RNMT-C or RNMT-C/RAM complexes show that RNMT-C cannot bind eIF4E

in the presence of RAM. **C.** Close up view of binding site of RAM for RNMT-C (PDB 5E8J) used to guide RNMT mutagenesis experiments. Only interactions with the first two helices of RAM were considered (the RNMT-C lobe binding site is not important for eIF4e association (Fig 1 G)). RNMT-C residues mutated are shown as sticks (single point mutants leading to a reduction in eIF4E binding are coloured red). **D.** GST pulldown assay between GST-eIF4E and wild type and mutant RNMT-C proteins. **E.** Lowest energy model of the complex of eIF4E with RNMT-C generated from Haddock. The catalytic site of RNMT (marked by SAH) and the cap-binding site of eIF4E are represented by arrows and far removed from the complex interface. **F, G.** Superposition of the Haddock generated model of eIF4E and RNMT-C with (**F**) RNMT-RAM coordinates (PDB ID 5E8J) and (**G**) the eIF4E-BP1 (PDB ID 3U7X) coordinates.

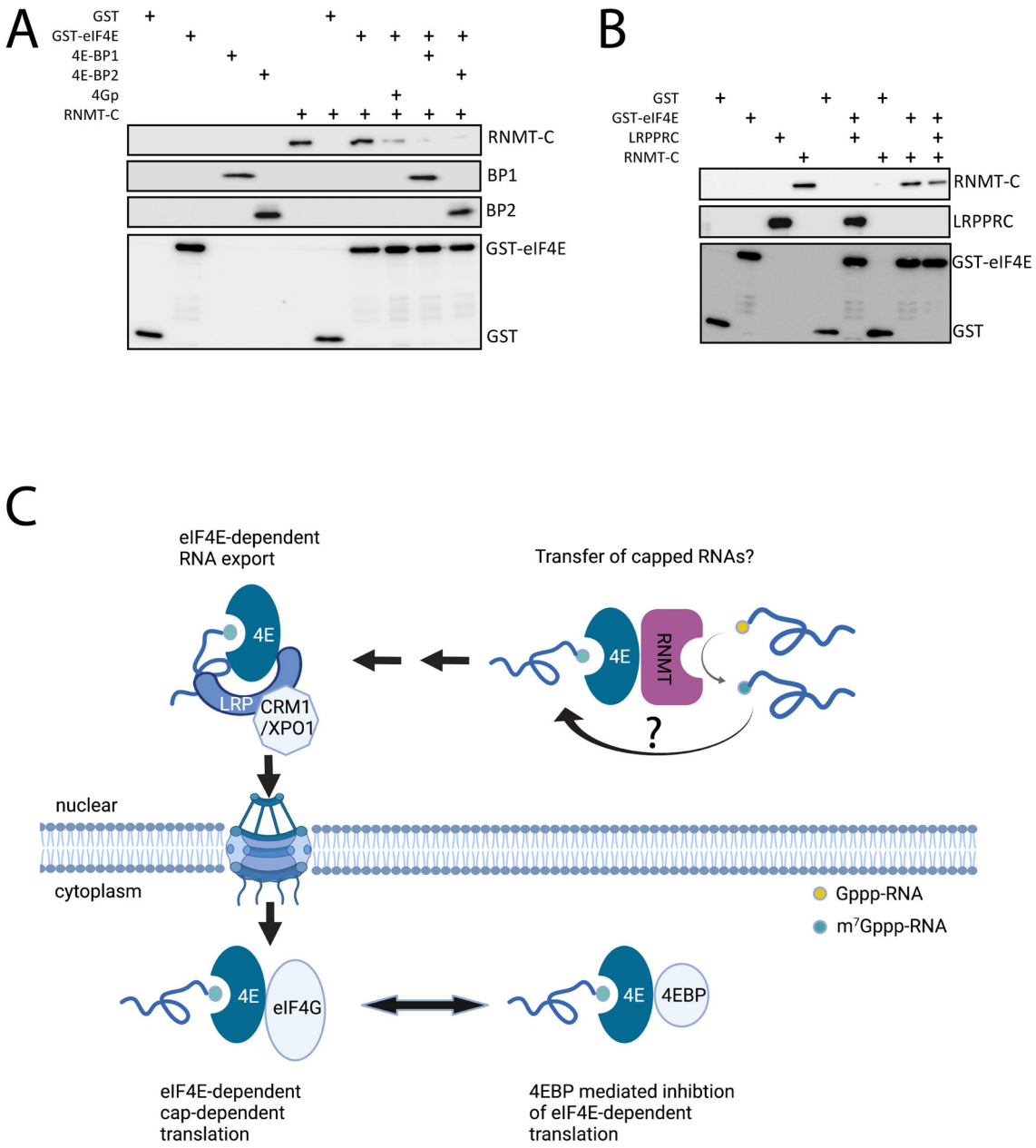

Figure 4. eIF4E-RNMT, eIF4E translation, and export complexes are mutually exclusive.

A, B. GST or GST-eIF4E pulldowns for RNMT-C in the presence or absence of 4E-BP1,4E-BP2, 4Gp (a peptide of eIF4G, see text) (**A**) or LRPPRC (**B**). Western blots are probed as indicated. Controls for GST binding are given in Supplementary Fig. S6. **C**. Schematic model of summarizing the complexes explored in A and B. RNMT, LRPPRC, eIF4G and the 4EBPs all bind overlapping surfaces on eIF4E and thus form mutually exclusive complexes. The multiple arrows between the RNMT and RNA export complexes indicate that there could be other complexes between the capping and export ones depicted. Not all eIF4E complexes known are shown here for simplicity.